

# Quasars: the characteristic spectrum and the induced radiative heating

S. Yu. Sazonov<sup>1,2\*</sup>, J. P. Ostriker<sup>3</sup> and R. A. Sunyaev<sup>1,2</sup>

<sup>1</sup>*Max-Planck-Institut für Astrophysik, Karl-Schwarzschild-Str. 1, 85740 Garching bei München, Germany*

<sup>2</sup>*Space Research Institute, Russian Academy of Sciences, Profsoyuznaya 84/32, 117997 Moscow, Russia*

<sup>3</sup>*Institute of Astronomy, Madingley Road, CB3 0HA Cambridge*

Accepted 2003 September 9. Received in original form 2003 May 14

## ABSTRACT

Using information on the cosmic X-ray background and the cumulative light of active galactic nuclei (AGN) at infrared wavelengths, the estimated local mass density of galactic massive black holes (MBHs) and published AGN composite spectra in the optical, UV and X-ray, we compute the characteristic angular-integrated, broad-band spectral energy distribution of the average quasar in the universe. We demonstrate that the radiation from such sources can photoionize and Compton heat the plasma surrounding them up to an equilibrium Compton temperature ( $T_C$ ) of  $2 \times 10^7$  K. It is shown that circumnuclear obscuration cannot significantly affect the net gas Compton heating and cooling rates, so that the above  $T_C$  value is approximately characteristic of both obscured and unobscured quasars. This temperature is above typical gas temperatures in elliptical galaxies and just above the virial temperatures of giant ellipticals. The general results of this work can be used for accurate calculations of the feedback effect of MBHs on both their immediate environs and the more distant interstellar medium of their host galaxies.

**Key words:** galaxies: active – quasars: general.

## 1 INTRODUCTION

Massive black holes (MBHs) at cosmological distances came to our attention more than three decades ago due to the enormous outflow from them of high energy radiation. This observed fact, combined with the inverse square law, implies that the immediate environs of these MBHs undergo dramatic heating (Levich & Sunyaev 1971) when they are in the luminous “on” state – radiating at rates approaching Eddington limit for their masses. Yet most work on active galactic nuclei (AGN) or the environment of MBHs has ignored this “feedback” effect, even though it is easy to demonstrate (e.g. Cowie, Ostriker & Stark 1978; Park & Ostriker 2001) that it should dramatically alter both the immediate environment of the MBH, from which accretion is occurring, and the more distant interstellar medium of the galaxy within which the MBH resides. The multiplicity of MBHs in the cores of galaxies found in groups and clusters may even sensibly alter the entropy floor of the ambient gas in these assemblages.

But an accurate calculation of all of these effects could not be made until we had accumulated and averaged the spectral output of representative samples of AGN – and that

data has been missing; the lack can now be remedied due to recent observational advances. Furthermore, some means needed to be found to perform the averages, due to strong variability of the sources with time, with viewing angle and from object to object.

It is the purpose of this paper to address these issues quantitatively: to compute the characteristic spectrum and all the important “Compton temperature”,  $T_C$ , of the average source and to estimate the consequences of exposing gas of cosmic chemical composition to the radiation from such sources. Specific applications of the general results of this paper will be presented in future publications. Jumping ahead to our conclusions, we constrain  $T_C$  to a narrow range around  $2 \times 10^7$  K. This estimate is based on 1) measurements of the cumulative AGN light at various wavelengths, 2) the measured local mass density of MBHs and 3) published composite quasar spectra. Interestingly, our estimate of the characteristic quasar Compton temperature is just above the virial temperatures of giant elliptical galaxies and somewhat below typical intracluster medium temperatures.

Before turning to our detailed calculation of quasar spectral output, it may be useful to present some additional background evidence and motivation. Comparison of the mass density of MBHs residing at the center of nearby galaxies with the total radiation flux from all AGN sug-

\* E-mail: sazonov@mpa-garching.mpg.de

gests that MBHs have grown by radiatively efficient accretion when their host galaxies were quasars. Overall radiation efficiencies [ $\epsilon_\gamma \equiv \Delta E_\gamma / (\Delta m_{\text{BH}} c^2)$ ] of  $\sim 0.1$ – $0.3$  are estimated (Fabian & Iwasawa 1999; Salucci et al. 1999; Elvis, Risaliti & Zamorani 2002; Yu & Tremaine 2002). It is important to note that this high mean efficiency is weighted by accretion rate; it is possible that during most of the lifetime MBHs accrete much less efficiently, but most of the mass must be accreted in (perhaps brief) high efficiency episodes.

Luminous quasars were much more abundant in the past (at redshifts  $\sim 2$ ) than at the current epoch and one may reasonably be puzzled as to why the most massive local ellipticals (such as M87), which contain the most massive black holes, are so quiescent. Elliptical galaxies do contain significant amounts of hot ( $\sim 10^7$  K) gas capable of accreting onto central MBHs due to its fast radiative cooling compared to the Hubble time. It has been suggested (Binney & Tabor 1995) that feedback from the MBH may regulate accretion from the ambient gas, leading to an oscillation-type behavior such that short periods of strong nuclear activity are interchanged with much longer quiescence periods during which the majority of observed galaxies are caught. This picture of brief intervals of high efficiency accretion separated by long periods of low level and low efficiency accretion is attractive in helping us understand the statistics of quasars and MBHs (Yu & Tremaine 2002).

Continuing this theme, Ciotti & Ostriker (1997, 2001) considered a scenario in which the gas of a central cooling flow is heated, during a quasar phase, above the galactic virial temperature by hard X-ray and gamma radiation from the MBH, which leads to a degassing of the central regions of the galaxy and switching off of the nucleus. A new episode of nuclear activity can begin after a large amount of cooled gas has again accumulated in the central regions of the galaxy. For this model to work, the characteristic quasar Compton temperature must be higher than the temperature of the cooling flow gas, otherwise the gas will be Compton cooled by the low-frequency radiation from the nucleus instead of being Compton heated. Regarding the Compton temperature as essentially a free parameter, Ciotti & Ostriker (2001) presented solutions for a number of  $T_C$  values ranging from  $5 \times 10^7$  to  $10^9$  K, and the results are qualitatively independent of  $T_C$  so long as  $c_C^2 = kT_C/m_p > v_*^2$ , the stellar velocity dispersion.

We note that the problem of gas preheating by X-rays emergent from MBHs finds its analogy in other astrophysical situations: near stellar-mass black holes located in globular clusters (Ostriker et al. 1976) as well as in X-ray binaries with stellar wind accretion onto a black hole or a neutron star (Sunyaev 1978).

## 2 BASIC ASSUMPTIONS AND CONSIDERATIONS

### 2.1 Obscured vs. unobscured AGN

In the standard AGN unification picture (Antonucci 1993), the active galactic nucleus is surrounded by an axisymmetric region (hereafter called the torus) filled with cold and dense material that intercepts and redistributes in wavelength and

direction a substantial fraction of the primary radiation. The source will be classified as an unobscured (type 1) or obscured (type 2) AGN if its nucleus is observed directly – at a small angle to the axis of symmetry, or through the torus, respectively. One can also imagine a different situation in which there are two physically different populations of sources: naked AGN (type 1) and AGN enshrouded in dense material (type 2). What plays the predominant role in nature, orientation or the presence/absence of a dense envelope, is still a matter of debate, but in either case type 1 and type 2 AGN exhibit distinctly different spectral energy distributions when observed far from the sources.

It turns out that although circumnuclear absorption definitely plays a crucial role in shaping the observed spectral energy distribution of quasar emission, its effect on the characteristic Compton temperature is expected to be small. To demonstrate this let us cast the usual definition of the Compton temperature (e.g. Levich & Sunyaev 1971) – the plasma temperature at which net energy exchange by Compton scattering between photons and electrons vanishes – in the following form:

$$kT_C = \frac{1}{4} \frac{\int_0^{10 \text{ keV}} E F_E dE + \int_{10 \text{ keV}}^\infty a(E) E F_E dE}{\int_0^{10 \text{ keV}} F_E dE + \int_{10 \text{ keV}}^\infty b(E) F_E dE}. \quad (1)$$

Here  $E$  is the photon energy,  $F_E(E)$  is the radiation spectral flux density, and the factors  $a(E)$  and  $b(E)$  represent Klein–Nishina corrections that become of importance in the hard X-ray regime (the corresponding explicit expressions are given in Appendix). Note that equation (1) is valid in the limit  $kT_C \ll m_e c^2 = 511$  keV; it becomes inaccurate by more than 5% at  $kT_C > 10$  keV (in general the expression for Compton energy exchange is nonlinear with respect to gas temperature, see e.g. Sazonov & Sunyaev 2001).

As will be detailed in §3 and §4, for the characteristic spectral output of a type 1 quasar the Compton heating rate is completely dominated by the high-energy integral  $\int_{10 \text{ keV}}^\infty a(E) E F_E dE$  while most of the Compton cooling is due to the component  $\int_0^{10 \text{ keV}} F_E dE$ . The latter integral represents energy flux integrated over the ‘blue bump’ and the infrared band. As a result, we may expect the estimate

$$kT_C \approx \frac{1}{4} \frac{\int_{10 \text{ keV}}^\infty a(E) E F_E dE}{\int_0^{10 \text{ keV}} F_E dE} \quad (2)$$

to be accurate to a few per cent for type 1 AGN.

If we now consider lines of sight passing through an obscuring torus, radiation emitted at  $E \gtrsim 10$  keV will be little affected by photoabsorption unless the torus is substantially Compton thick:  $N_{\text{H}} > \text{a few } 10^{24} \text{ cm}^{-2}$ . Further, most of the radiation emitted at  $E \lesssim 10$  keV will be absorbed and reemitted in the infrared, approximately retaining the total radiation flux due to energy conservation. Thus, neither the numerator nor the denominator of the RHS of equation (2) is affected by obscuration to first order and we may expect that equation (2) with  $F_E$  representing as before the characteristic type 1 spectrum will also be a good approximation for the characteristic Compton temperature of type 2 AGN.

The above line of argument is directly applicable to the scenario with two populations of sources, the unobscured and the obscured. On the other hand, orientation-based unification schemes assume that an obscuring torus is present in

all AGN but it covers a solid angle of less than  $4\pi$ . In the case of such geometry, observers in unobscured directions will receive both direct emission from the nucleus and a similar flux of reprocessed infrared radiation from the torus. As a result, the characteristic Compton temperatures of type 1 and type 2 AGN could be somewhat lower and higher, respectively, than the angular averaged  $T_C$  given by equation (2).

We conclude that the characteristic Compton heating and cooling rates (per particle) should be the same within a factor of  $\sim 2$  in all directions at a given distance from the AGN if the spectral distribution of primary emission is isotropic. This implies that knowledge of the angular averaged spectral output of a typical quasar would make it possible to calculate with good precision the effect of Compton heating/cooling of gas around quasars. We note, however, that other radiative mechanisms such as photoionization heating and line cooling do depend strongly on the degree of circumnuclear absorption (see §5.2).

On the other hand, it is reasonable to expect that the two main spectral components of the intrinsic AGN radiation, the blue bump and the hard X-ray component, have somewhat different angular distributions. This will of course influence the ratio of the heating and cooling rates in equation (2). Since one of the main goals of this work is to obtain an unbiased estimate of the characteristic Compton temperature of the average quasar, we will give more weight in our computations to data on cumulative AGN light, such as the cosmic X-ray background and the total infrared flux from all AGN, than to another valuable source of information – composite spectra of type 1 quasars. The latter probably represent a snapshot of quasar emission in a certain cone of angles or/and from a certain population of objects.

## 2.2 Cumulative AGN light

As mentioned above, our derivation of the spectral output of the average quasar (in §3) will be primarily based on measurements of cumulative AGN light from the sky. It will be based on the standard procedure described below.

Let  $\epsilon_E(E, z)$  ( $\text{erg s}^{-1} \text{cm}^{-3} \text{keV}^{-1}$ ) be the angular integrated spectral emissivity of AGN in a unit comoving volume of the universe at redshift  $z$ . Then AGN located in the redshift interval  $[z, z + dz]$  will contribute to the locally measured surface brightness of the sky the amount

$$dI_E(E) = \frac{c}{4\pi} \epsilon_E(E', z) \left| \frac{dt}{dz} \right| dz \quad (\text{erg s}^{-1} \text{cm}^{-2} \text{sr}^{-1} \text{keV}^{-1}), \quad (3)$$

where  $t$  is the cosmic time and  $E' = E(1+z)$  is the energy a detected photon had when it was emitted.

Integrating equation (3) over redshift gives the intensity of cumulative AGN light:

$$I_E(E) = \frac{c}{4\pi H_0} \int_0^\infty \frac{\epsilon_E((1+z)E, z) dz}{(1+z) [\Omega_M (1+z)^3 + \Omega_\Lambda]^{1/2}}. \quad (4)$$

We adopt the concordance model cosmology (Ostriker & Steinhardt 1995):  $\Omega_M = 0.3$  and  $\Omega_\Lambda = 0.7$ . Assuming that there is no spectral evolution of AGN with redshift, we may further write

$$\epsilon_E(E, z) = \langle F_E(E) \rangle e(z). \quad (5)$$

Here, the function  $e(z)$  describes the evolution with redshift of the AGN comoving volume emissivity.

Equations (4) and (5) establish the relation between the measurable spectral energy distribution of the cumulative AGN light,  $I_E(E)$ , and the angular integrated spectral output of the average quasar,  $\langle F_E(E) \rangle$ , that we wish to determine and which characterizes the global energy release via accretion onto MBHs.

The volume emissivity of type 1 quasars reaches a maximum at  $z_{\text{max}} \sim 2$  (e.g. Schmidt, Schneider & Gunn 1995). Therefore, if the cumulative spectrum  $I_E(E)$  were known, one could roughly estimate  $\langle F_E(E) \rangle$  simply by shifting  $I_E(E)$  to higher energies:  $E \rightarrow (1+z_{\text{max}})E$ . A more accurate treatment must be based on equations (4) and (5) and requires the knowledge of the evolution function  $e(z)$ . We adopted the following evolution law in our computations:

$$e(z) = \begin{cases} (1+z)^3, & z \leq z_0 \\ e(z_0) \exp(z_0 - z), & z > z_0 \end{cases} \quad (6)$$

$$z_0 = 2.5.$$

We have also considered the alternative law

$$e(z) = \begin{cases} (1+z)^3, & z \leq z_0 \\ e(z_0), & z > z_0, \end{cases} \quad (7)$$

We shall see (in §3.1) that both types of evolution lead to practically the same results that are almost insensitive to the value of the critical redshift if  $z_0 \gtrsim 2$ .

The above parametrization is motivated by the following data. The evolution of type 1 quasars detected in the 2dF and Sloan Digital Sky optical surveys (Boyle et al. 2000; Fan et al. 2001) approximately matches the cutoff pattern, equation (6), with  $z_0 = 2.5$ . *ROSAT* soft X-ray (0.5–2 keV, Miyaji, Hasinger & Schmidt 2000) and *BeppoSAX* hard X-ray (2–10 keV, La Franca et al. 2002) surveys suggest that type 1 quasars evolve approximately following equation (7) with  $z_0 = 1.5$ . The blazars observed at gamma-rays (above 20 MeV) with *CGRO/EGRET* evolve as  $e(z) \propto (1+z)^3$  up to at least  $z \sim 2$ , with no data available for higher redshift (Chiang & Mukherjee 1998).

The most recent *Chandra* deep X-ray (0.5–2 keV) and hard X-ray (2–8 keV) observations have confirmed a decline in the number density of quasars at  $z > 3$  but additionally revealed a second peak in source counts at  $z = 0.5$ –1 (Hasinger 2003; Cowie et al. 2003). This low-redshift peak is, however, dominated by Seyfert galaxies, both unobscured and obscured, with X-ray luminosities in the range  $L_X = 10^{42}$ – $10^{44} \text{erg s}^{-1}$ , as compared to the previously known  $z \sim 2$  maximum in the number density of quasars with  $L_X \gtrsim 10^{44} \text{erg s}^{-1}$ . For this reason, the low-redshift peak is less prominent in terms of the contribution to the total AGN X-ray light – in fact about a third of the cosmic X-ray background is now believed to come from AGN at  $z < 1$  (Barger et al. 2002). This could move the redshift of a typical AGN contributing to the cumulative AGN light from  $\langle z \rangle \approx 1.5$  (see §3.1) to  $\langle z \rangle \approx 1$  but unlikely to lower redshift. Since the relevant redshift correction factor is  $1 + \langle z \rangle$ , the inferred average quasar spectrum could change by some 25%. Considering this correction unimportant in view of the remaining uncertainties on the observational side, we ignore the  $z \approx 0.7$  peak altogether in our calculations.

### 3 THE SPECTRAL OUTPUT OF THE AVERAGE QUASAR

In this section we construct the average quasar spectrum from its pieces corresponding to different energy bands.

#### 3.1 High-energy emission

We first consider emission above 2 keV. This spectral region is the main contributor to the Compton heating by quasars. It is now well established that the bulk of the cosmic X-ray and gamma-ray background (hereafter CXGB), the observed spectrum of which is shown in Fig. 1, is composed of contributions from AGN of varying degree of obscuration, luminosity and radio loudness (Madau, Ghisellini & Fabian 1994; Comastri et al. 1995; Gilli, Salvati & Hasinger 2001). This conclusion is based on 1) X-ray source counts, with some 80% of the  $E < 5$  keV background having been resolved into discrete sources (Hasinger et al. 2001; Rosati et al. 2002), 2) data on the hard X-ray spectra of Seyfert galaxies, 3) the measured distribution of absorbing column densities in Seyferts (Risaliti, Maiolino & Salvati 1999), 4) the redshift evolution of quasars and 5) for the gamma-ray part tentatively also on the observed similarity of the slopes of the CXGB spectrum and the spectra of EGRET blazars (Sreekumar et al. 1998).

This allows us to identify, with some reservations as noted below (in §3.1.2 and §3.1.3), the CXGB with the cumulative AGN spectrum  $I_E(E)$  and estimate the high-energy part of the average quasar spectrum  $\langle F_E \rangle$  using the equations of §2.2.

The CXGB spectrum was reliably measured in the 3–400 keV and 2 MeV–100 GeV bands by the *HEAO-1* and *CGRO* observatories, and a useful formula fitting the measured intensities was proposed by Gruber et al. (1999). The spectrum peaks (when plotted in units  $E I_E$ , see Fig. 1) at  $\sim 30$  keV, is characterized by an approximately constant slope ( $I_E \propto E^{-\alpha}$ )  $\alpha \approx 0.3$  at  $\lesssim 20$  keV, by a varying slope  $\alpha \sim 1.5$  at energies above the peak up to  $\sim 10$  MeV and is approximately a power law with  $\alpha \approx 1.1$  at higher energies.

Extrapolating the Gruber et al. formula for the CXGB spectrum down to 1 keV, we find  $I_E(1 \text{ keV}) = 8 \text{ keV s}^{-1} \text{ cm}^{-2} \text{ sr}^{-1} \text{ keV}^{-1}$ , which is 20% below but is marginally consistent with the newest estimate based on all-sky observations with RXTE/PCA (Revnivtsev et al. 2003) and similarly below the value derived from a joint analysis of *ROSAT* and *ASCA* observations of small celestial fields (Miyaji et al. 1998), the latter estimate being affected by cosmic variance. We thus apply the Gruber et al. fitting formula to describing the CXGB spectrum at all energies above 1 keV, except for the poorly explored 0.4–2 MeV region which we omit from our analysis, and adopt a 20% uncertainty in the CXGB normalization.

We next adopt the template quasar spectrum

$$\begin{aligned} \langle F_E \rangle &= A \begin{cases} E^{-\alpha} e^{-E/E_1}, & 2 \text{ keV} \leq E < E_0 \\ B (1 + kE^{\beta-\gamma}) E^{-\beta}, & E \geq E_0 \equiv (\beta - \alpha) E_1 \end{cases} \\ A &= 2^\alpha e^{2/E_1}, \quad B = E_0^{\beta-\alpha} e^{-(\beta-\alpha)} / (1 + kE_0^{\beta-\gamma}) \\ \alpha &= 0.24, \quad \beta = 1.60, \quad \gamma = 1.06 \\ E_1 &= 83 \text{ keV}, \quad k = 4.1 \times 10^{-3}. \end{aligned} \quad (8)$$

The spectrum  $E \langle F_E \rangle$  is shown in Fig. 1; it peaks at ap-

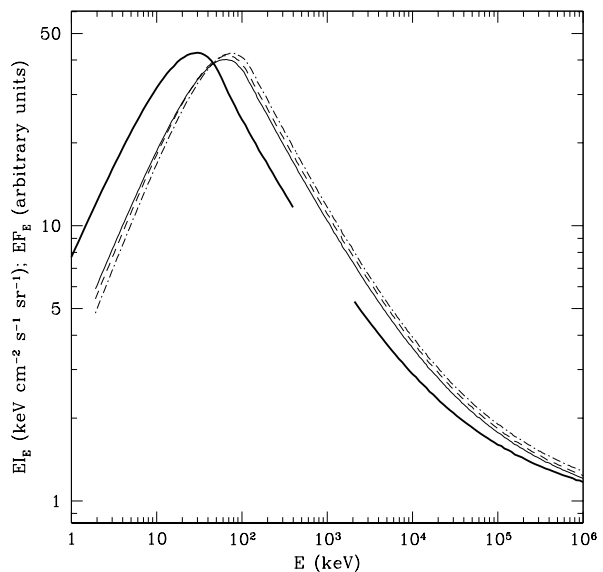


**Figure 1.** Measured CXGB spectrum (heavy solid line with a gap) and the adopted, rest-frame high-energy spectrum of the average quasar, equation (8) (solid line). The redshifted light from a population of such quasars distributed in redshift according to equation (6) has a spectral distribution that fits well the CXGB spectrum. For comparison shown are two other source templates, which generate similarly good fits to the CXGB spectrum when assuming different evolution scenarios: equation (6) with  $z_0 = 3$  (dashed line) and equation (7) with  $z_0 = 2.5$  (dash-dotted line).

proximately 60 keV. The convolution of this average spectrum with the evolution law given by equation (6) provides an excellent fit to the CXGB spectrum. We note that the characteristic slopes of the template (8) in different spectral regions are nearly the same as the corresponding original values for the CXGB spectrum. This reflects the fact that only templates of the type (8) can lead to the observed CXGB spectrum; essentially only the position of the peak is found from the fit. The high-energy template (8) is normalized so that  $\langle F_E \rangle(2 \text{ keV}) = 1$ . Our choice for the lower boundary of the spectrum (2 keV) is motivated by the expectation that obscured sources contribute negligibly to the average quasar spectrum at  $\lesssim 2$  keV and also by the fact that the high-energy component and the UV–soft X-ray component that will be discussed in §3.2 join near 2 keV in type 1 quasar spectra (Laor et al. 1997).

Repeating the same fitting procedure for  $z_0 = 3$  or assuming the evolution given by equation (7) with  $z_0 = 2.5$ , we obtain average spectra that deviate from the previous one by less than 10% (see Fig. 1). This demonstrates a very weak dependence of the result on the assumed evolution scenario at  $z > 2.5$ , which reflects the fact that a typical quasar contributing to our average spectrum is located at  $\langle z \rangle = 1.3$ –1.8 (depending on  $E$ ). Emission from substantially higher redshifts contributes little to the background.

### 3.1.1 The average spectrum as a sum of the spectra of obscured and unobscured sources

One can see that the average quasar spectrum just derived differs notably below a few tens keV from observed X-ray spectra of both unobscured and obscured AGN. This is, however, consistent with this spectrum being the result of averaging over sources with a range of line-of-sight photoabsorption columns. To illustrate this point and also for the purposes of our further radiative energy exchange computations, let us introduce two additional spectra of which one will be representative of the spectra of type 1 quasars and the other will characterize their obscured counterparts. We impose the requirement that the appropriately weighted sum of these two spectra should match well the globally averaged one. We exclude from the current consideration blazars, assuming that they do not contribute significantly to the average spectra below  $\sim 500$  keV, as will be justified in §3.1.2.

Most of the published information on AGN X-ray spectra pertains to nearby ( $z \ll 0.1$ ), relatively low-luminosity ( $L_X = 10^{42}$ – $10^{44}$  erg s $^{-1}$ , the unabsorbed luminosity in the 2–10 keV band) Seyfert 1 and Seyfert 2 galaxies. Perola et al. (2002) have recently presented a sample of broad-band (0.1–200 keV) spectra obtained with the BeppoSAX satellite for nine Seyfert 1s with  $L_X$  ranging from  $5 \times 10^{42}$  to  $10^{44}$  erg s $^{-1}$ . The measured spectral continua above a few keV are well fitted by a model consisting of a power law with high-energy exponential cutoff,  $E^{-\alpha} \exp(-E/E_f)$ , and a Compton reflection component. Typical values for the power-law index are  $\alpha \approx 0.8$  and the cutoff energies  $E_f$  span from about 70 keV to more than 300 keV, typically  $E_f \sim 200$  keV. The relative amplitude of the reflection component attributed to a weakly ionized accretion disk is  $R = 0.5$ – $1$ . The above values of  $E_f$  are somewhat lower than the previous estimates ( $E_f \gtrsim 250$  keV) based on *EXOSAT*, *GINGA*, *HEAO-1* and *CGRO/OSSE* data (Gondek et al. 1996). We note that a rollover at  $\sim 50$ – $100$  keV was first clearly detected in the spectrum of NGC 4151 with *GRANAT/SIGMA* (Jourdain et al. 1992).

A separate well-studied class of AGN is radio galaxies, which can be considered the radio-loud counterparts of Seyfert galaxies. Their X-ray spectra are similar to those of Seyferts, i.e.  $\alpha \approx 0.8$ ,  $E_f \gtrsim 100$  keV, except that the reflection component seems to be weaker and is actually undetected in most cases (Woźniak et al. 1998; Eracleous, Sambruna & Mushotzky 2000; Grandi, Urry & Maraschi 2002). Note that the studied radio galaxies are on average more luminous ( $L_X \sim$  a few  $10^{44}$  erg s $^{-1}$ ) than the Seyferts discussed above.

On the other hand, the available information on luminous ( $L_X \gtrsim 10^{44}$  erg s $^{-1}$ ) AGN located at  $z > 0.1$ , which usually are classified as quasars, is rather scarce and generally limited to  $E < 20$  keV. However, the AGN X-ray luminosity function is characterized by an increasing typical luminosity  $L_*$  with redshift, so that  $L_*(z < 1) \sim$  a few  $\times 10^{43}$  erg s $^{-1}$  while  $L_*(z > 1) \sim$  a few  $\times 10^{44}$  erg s $^{-1}$  (Miyaji, Hasinger & Schmidt 2000; Cowie et al. 2003). As a consequence, a typical AGN contributing to the CXGB is a quasar at  $z \sim 1$ – $2$  with a luminosity  $L_X \gtrsim 10^{44}$  erg s $^{-1}$ .

All of the available information on quasars (excluding blazars) is consistent with their X-ray spectral continua being very similar to those of local Seyfert and ra-

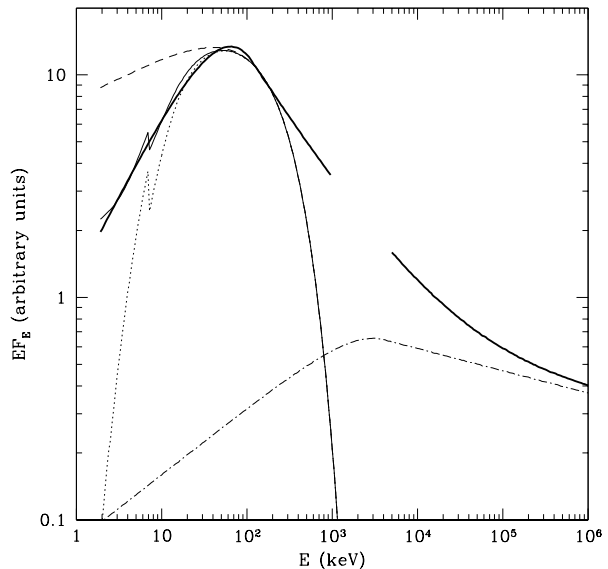


**Figure 2.** Heavy solid line: Adopted high-energy spectrum of the average quasar, equation (8), with the gap at 1–5 MeV approximately corresponding to the 0.4–2 MeV poorly explored region in the CXGB spectrum (see Fig. 1). Dashed line: Adopted spectrum of the average unobscured quasar, equation (9). Dotted line: Adopted spectrum of the average obscured quasar, equations (10) and (11). Note that above  $\sim 50$  keV the obscured and unobscured spectra coincide because photoabsorption becomes negligible. Solid line: Weighted sum, equation (12), of the average obscured and unobscured spectra. Dash-dotted line: Estimated upper limit, equation (13), on the contribution of blazar emission to the average quasar spectrum.

dio galaxies. In particular, the 1–20 keV spectra of both radio-quiet and radio-loud type 1 quasars are characterized by  $\alpha \approx 0.8$  (Lawson & Turner 1997; Reeves & Turner 2000; Hasenkopf, Smabruna & Eracleous 2002). In addition, high-energy spectral cutoffs with  $E_f \sim 100$  keV have been reported for at least two nearby ( $z \sim 0.1$ ) quasars, PG 1416–129 and MR 2251–178 (Staubert & Maisack 1996; Orr et al. 2001). It appears that the Compton reflection component is generally weak at least in the most luminous quasars with  $L_X \sim 10^{46}$  erg s $^{-1}$  (Reeves & Turner 2000).

Summarizing the above facts, we adopt the following spectrum (plotted in Fig. 2) for the average unobscured quasar:

$$\langle F_E \rangle (\text{type1}) \propto E^{-0.8} e^{-E/200 \text{ keV}}. \quad (9)$$

The chosen value for the cutoff energy not only falls comfortably in the range of  $E_f$  values found for nearby AGN and quasars, but also leads to the right location of the peak in our globally averaged quasar spectrum. We also note that the addition of a  $R \sim 0.5$  reflection component to equation (9) would have a fairly similar effect on the spectrum as slightly modifying the main parameters –  $\alpha \approx 0.7$  and  $E_f \approx 150$  keV. Since such changes are within the current observational uncertainties and of the same order as source-to-source variations, we ignore the reflection component. We

also ignore the usually observed fluorescence  $K_\alpha$  iron line, since its equivalent width is small ( $\sim 100$  eV, the above references).

We next introduce another spectrum, which we attribute to the average obscured quasar:

$$\langle F_E \rangle(\text{type2}) = \langle F_E \rangle(\text{type1}) \times \int f(N_{\text{H}}) \exp[-\sigma(E)N_{\text{H}}] dN_{\text{H}}, \quad (10)$$

where  $\sigma(E)$  represents the photoelectric absorption cross section for solar chemical composition (Morrison & McCammon 1983). We adopt a lognormal distribution of absorption columns centered at  $N_{\text{H}} = 10^{24} \text{ cm}^{-2}$ :

$$f(\log N_{\text{H}}) = \frac{1}{\sqrt{\pi}} \exp[-(\log N_{\text{H}} - 24)^2]. \quad (11)$$

Our choice of the central value for  $f(\log N_{\text{H}})$  is in first place dictated by the shape of the globally averaged quasar spectrum at  $E \lesssim 50$  keV, which is much flatter than the unabsorbed spectrum (9). In addition, the median value of the inferred  $N_{\text{H}}$  distribution for the local population of Seyfert 2s is  $\sim 10^{24} \text{ cm}^{-2}$  (Risaliti et al. 1999). The width of the  $N_{\text{H}}$  distribution, equation (11), was taken just sufficiently large to produce a relatively smooth spectrum. For simplicity, we neglect here the Compton scattering of nuclear radiation in the obscuring torus, which can significantly modify the emergent spectrum when  $\log N_{\text{H}} \gtrsim 24.5$  (Matt, Pompilio & La Franca 1999).

The absorbed spectrum given by equations (10) and (11) is shown in Fig. 2. We should mention that X-ray spectra exhibiting a low-energy exponential cut-off have been recently measured for several obscured quasars (Iwasawa, Fabian & Etori 2001; Stern et al. 2002; Norman et al. 2002).

Finally, we demonstrate in Fig. 2 that our globally averaged quasar spectrum is well fit below  $\sim 300$  keV by a weighted sum of the adopted average spectra of type 1 and type 2 quasars:

$$\langle F_E \rangle \approx 0.25 \langle F_E \rangle(\text{type1}) + 0.75 \langle F_E \rangle(\text{type2}). \quad (12)$$

This corresponds to the ratio 3 : 1 of obscured to unobscured sources, similar to that (4 : 1) estimated for the local population of Seyfert galaxies (Maiolino & Rieke 1995).

### 3.1.2 Contribution from blazars

Although there is little doubt that in the 2–300 keV band our adopted average quasar spectrum represents mostly normal, nonblazar quasar emission, the situation is more uncertain in the gamma-ray region where blazars and non-AGN sources may contribute to the average spectrum inferred from the CXGB.

According to a popular view (e.g. Zdziarski 1996), the CXGB above a few MeV is to a large part due to blazars, an AGN class which we excluded from our consideration in §3.1.1. The spectra of blazars are believed to be dominated by Doppler boosted radiation from a relativistic jet pointing close to our line of sight (e.g. Urry & Padovani 1995), as compared to the quasi-isotropic emission from normal quasars. Regardless of whether powerful jet emission is produced in most quasars but is usually beamed away from us,

or it occurs only in a small fraction of them, obviously it is important to estimate the contribution of blazar emission to the average quasar spectrum. As we shall demonstrate in §4 using a constraint obtained below, blazar beamed emission is at best a minor contributor to the global AGN energy output as well as to the global radiative heating by AGN.

In contrast to normal quasars, it proves impossible to produce any meaningful average spectrum for blazars, since blazar spectra vary dramatically from object to object and also with time: they usually consist of two broad peaks, whose positions and relative amplitudes vary by orders of magnitude (e.g. Fossati et al. 1998). Nonetheless, we can still derive an interesting upper limit on the expected contribution from blazars to the average quasar spectrum using the following facts:

(i) The 30 MeV–10 GeV spectra of some 50 blazars detected by *CGRO*/EGRET are consistent with being simple power laws, with the average energy index  $\alpha \approx 1.15 \pm 0.04$  (Mukherjee et al. 1997), which is equal within the errors to the slope ( $\alpha \approx 1.10 \pm 0.03$ ) of the CGRB spectrum in the 30 MeV–100 GeV range (Sreekumar et al. 1998).

(ii) An estimated luminosity function of gamma-ray blazars and its evolution, combined with the spectral information above, suggest that blazars contribute at least a significant fraction of the CXGB in the EGRET energy range (Chiang & Mukherjee 1998; Sreekumar et al. 1998).

(iii) The spectra of gamma-ray blazars peak at MeV energies (Schönfelder 1994; McNaron-Brown et al. 1995).

(iv) The spectral slopes of gamma-ray blazars measured between 2 keV and a few  $\times 10^2$  keV vary considerably from object to object but tend to group around  $\alpha \approx 0.7$  (McNaron-Brown et al. 1995; Kubo et al. 1998; Tavecchio et al. 2002).

(v) The contribution of all types of radio-loud quasars to the CXGB background in the  $\sim 1$  keV range is  $\lesssim 10\%$  (della Ceca et al. 1994), and the contribution of blazars, though very uncertain, is likely several times lower,  $\sim 1\%$  (Comastri, Di Girolamo & Setti 1996).

The following spectrum (see Fig. 2) therefore provides a plausible upper limit on the contribution of blazar emission to the average quasar spectrum:

$$\langle F_E \rangle(\text{blaz}) = \begin{cases} 0.082E^{-0.7} e^{-E/10^4 \text{ keV}}, & 2 \text{ keV} \leq E < 4 \text{ MeV} \\ 1.52E^{-1.1}, & E \geq 4 \text{ MeV}. \end{cases} \quad (13)$$

The spectrum (13) was obtained by fixing the lower-energy and high-energy slopes at  $\alpha = 0.7$  and 1.1, respectively, and also assuming that the blazar contribution to the globally averaged spectrum is 5% at 2 keV and  $\approx 100\%$  at  $> 100$  MeV. These conditions uniquely determine the characteristic break energy.

### 3.1.3 Contamination by other types of sources

The largest uncertainty is associated with the 300 keV–10 MeV part of the average spectrum (see Fig. 2). First, we essentially do not know the intensities at 1–5 MeV (see Fig. 2) since the CXGB has not been reliably detected in the corresponding 400 keV–2 MeV band (here we assume that a typical source contributing to the CXGB is at  $z \sim 1.5$ ). Moreover, other types of astrophysical sources, not necessarily AGN, may provide the major contribution in this

energy range. The most promising candidate proposed so far is Type 1a supernovae (The, Leising & Clayton 1993; Ruiz-Lapuende, Cassé & Vangioni-Flam 2001). Finally, it cannot be ruled out that a subclass of blazars exhibiting a peculiar spectral bump at  $\sim 1$  MeV may provide a significant contribution (Blom et al. 1995; Comastri et al. 1996). The last hypothesis remains highly speculative at present, since only a few such “MeV blazars” have been observed.

Fortunately, although the uncertainty associated with the average quasar spectrum above 300 keV is large, it cannot affect significantly our estimates of the global heating and cooling rates by AGN (see §4).

### 3.2 Near-infrared to soft X-ray emission

We next consider the 1 eV–2 keV band (which corresponds to wavelengths  $\lambda$  from 1.2  $\mu\text{m}$  to 6  $\text{\AA}$ ). Since there are practically no data on cumulative AGN light for this spectral range, our approach below will be different than in the preceding section.

In the standard AGN unification scenario, an obscuring torus of dust and gas with  $N_{\text{H}} \sim 10^{22}\text{--}10^{24}$   $\text{cm}^{-2}$  will be transparent to X-rays above  $\sim 10$  keV and also to infrared and low-frequency radiation at  $\lambda \gtrsim 10$   $\mu\text{m}$ . All the near-infrared to soft X-ray radiation emitted by the nucleus along obscured lines of sight will be absorbed and reemitted at IR and submillimeter wavelengths. We may thus expect that the spectrum of the average quasar at 1 eV–2 keV will be completely dominated by emission from unobscured sources. We can therefore take advantage of the ample existing information on type 1 quasar spectra, which we may condense in the simple spectral form

$$\langle F_E \rangle = 1.20 \begin{cases} 159E^{-0.6} & 1 \text{ eV} \leq E < 10 \text{ eV} \\ E^{-1.7}e^{E/2 \text{ keV}} & 10 \text{ eV} \leq E < 2 \text{ keV}. \end{cases} \quad (14)$$

Here 10 eV approximately corresponds to  $\lambda_{\text{Ly}\alpha} = 1216$   $\text{\AA}$  and the adopted normalization is such that the combined spectrum given by equations (8) and (14) is continuous at 2 keV.

In deriving equation (14), we took into account miscellaneous recently published data on quasars, including the Hubble Space Telescope catalog of UV spectra (Telfer et al. 2002), composite optical–UV spectra from the Sloan Digital Sky Survey (SDSS, Vanden Berk et al. Vanden Berk et al. 2001), 0.2–2 keV spectra from the *ROSAT* Bright Quasar Survey (Laor et al. 1997), and statistics on the characteristic 2500  $\text{\AA}$ –2 keV spectral slope,  $\alpha_{\text{OX}}$  (Yuan et al. 1998; Vignali, Brandt & Schneider 2003). We also used the atlas of quasar energy distributions of Elvis et al. (1994). We note that the combined contribution of resolved emission lines, including Ly $\alpha$ , to the total luminosity of the blue bump dominated by the continuum is small (Telfer et al. 2002), but nevertheless an attempt has been made to take it into account in the definition (14).

The  $\alpha_{\text{OX}}$  index is particularly relevant for our study, since it together with the spectrum of the hard X-ray component determines the ratio of the amplitudes of the hard X-ray and blue bumps in the quasar spectrum. Equation (14) yields  $\alpha_{\text{OX}} = 1.4$ . For comparison, the Elvis et al. (1994) mean radio-quiet and radio-loud quasar spectra are characterized by  $\alpha_{\text{OX}} = 1.4$  and  $\alpha_{\text{OX}} = 1.3$ , respectively.

From analysis of optical and *ROSAT*, *Chandra* and *XMM-Newton* X-ray data for optically selected SDSS quasars (with redshifts up to 6), Vignali et al. (2003) have inferred a dependence of  $\alpha_{\text{OX}}$  on quasar rest-frame UV luminosity:  $\alpha_{\text{OX}} \approx 1.5$  for  $L_{2500 \text{ \AA}} \sim 10^{30}$   $\text{erg s}^{-1}$   $\text{Hz}^{-1}$  and  $\approx 1.7$  for  $L_{2500 \text{ \AA}} \sim 10^{32}$   $\text{erg s}^{-1}$   $\text{Hz}^{-1}$ . We note that these monochromatic luminosities correspond to  $L_{2\text{--}10 \text{ keV}}$  ranging from  $\sim 10^{44}$  to  $\sim 10^{46}$   $\text{erg s}^{-1}$  and, as was noted in §3.1, the lower values from this range are characteristic of the quasars producing the bulk of the global AGN energy output, suggesting that  $\alpha_{\text{OX}} \approx 1.5$  might be a typical value globally.

We note that the template given by equation (14) possesses a number of key properties of observed quasar spectra, including a turnover near  $\lambda_{\text{Ly}\alpha}$  (Telfer et al. 2002) and a gradual flattening in the 0.2–2 keV band. The adopted template, primarily inferred from recent UV observations, is redder than the ‘big blue bump’ predicted by most theoretical accretion disk models whose spectra extend to the extreme ultraviolet (see Koratkar & Blazé 1999 for a review). We should also note that the spectra of radio-quiet and radio-loud quasars are quite similar up to  $\sim 100$  eV (Elvis et al. 1994), with  $\approx 90\%$  of all quasars being radio quiet and this fraction being seemingly independent of redshift and bolometric luminosity (Stern et al. 2000; Ivezić et al. 2002; see however Cirasuolo et al. 2003).

Given the remaining uncertainty in the  $\alpha_{\text{OX}}$  value characterizing the globally averaged quasar spectral output, we estimate that the ratio of the optical–UV to high-energy integrated radiation fluxes that follows from equations (8) and (14) for the average quasar spectrum is uncertain by a factor of  $\sim 2$ .

We note that recent data seem to indicate that the scatter in the near-IR to soft X-ray spectrum from quasar to quasar is fairly small. Indeed, according to the Hubble Space Telescope observations (Telfer et al. 2002) the blue bump peaks invariably at  $\lambda \approx 1200$   $\text{\AA}$  (i.e. not far from 2500  $\text{\AA}$ , the wavelength appearing in the definition of  $\alpha_{\text{OX}}$ ) for quasars whose monochromatic luminosities  $\nu L_{\nu}$  at 1100  $\text{\AA}$  range from a few  $10^{45}$  to a few  $10^{47}$   $\text{erg s}^{-1}$  (which corresponds to  $L_{2\text{--}10 \text{ keV}}$  ranging from  $\sim 10^{44}$  to  $\sim 10^{46}$   $\text{erg s}^{-1}$ ). On the other hand, the rms scatter in  $\alpha_{\text{OX}}$  for a given luminosity is of the order of 0.1 (Vignali et al. 2003), which corresponds to a factor of 2 scatter in the ratio  $\nu L_{\nu}(2 \text{ keV})/\nu L_{\nu}(1200 \text{ \AA})$ , which is similar to our estimated uncertainty in this ratio for the average spectrum.

### 3.3 Medium-infrared to submillimeter emission

Finally, we consider the spectral range  $\lambda > 1$   $\mu\text{m}$ , a major contributor to the net Compton cooling. As for the high-energy region, both obscured and unobscured sources are expected to significantly contribute to the integrated AGN light at IR and submm wavelengths. Although there is only fragmentary information on  $I_E(E)$  in this case, we shall use it below to derive some constraints on the average quasar spectrum at  $\lambda > 1$   $\mu\text{m}$ . There remains, after all available observations are utilized, a substantial uncertainty in the medium-IR luminosity of a typical quasar. However, as will be noted and demonstrated below, we have an integral constraint that provides an additional strong bound. The total luminosity of all quasars is limited by the observed, low-

redshift density of MBHs. This limits the integrated low-frequency emission.

Our approach will be similar to several previous studies of the contribution of AGN to the cosmic IR and submm background (hereafter CIB, Almaini, Lawrence & Boyle 1999; Risaliti, Elvis & Gilli 2002). We take into account the following data and limits related to the cumulative IR quasar light:

(i) The CIB spectrum (after subtraction of the cosmic microwave background) at 125–2000  $\mu\text{m}$  measured by the COBE/FIRAS experiment (Fixsen et al. 1998).

(ii) Luminous AGN, which produce the bulk of the cosmic X-ray background, contribute less than 10% to the CIB background at 850  $\mu\text{m}$ , as inferred from the cross-correlation of SCUBA submm sources with *Chandra* deep X-ray surveys (Severgnini et al. 2000; Fabian, Smail & Iwasawa 2000).

(iii) The CIB at 15  $\mu\text{m}$ :  $EI_E(15 \mu\text{m}, \text{total}) \approx 3 \text{ nW m}^{-2} \text{ sr}^{-1}$  (Franceschini et al. 2001; Elbaz, Cesarsky & Chantal 2002), and  $\approx 17\%$  of this intensity is due to AGN that make up  $\sim 85\%$  of the 2–10 keV background, as inferred from the cross-correlation of *XMM-Newton* and *Chandra* deep X-ray surveys with ISOCAM infrared surveys (Fadda, Flores & Hasinger 2002). One can thus estimate the cumulative quasar mid-IR light as  $EI_E(15 \mu\text{m}) = 0.5 \pm 0.15 \text{ nW m}^{-2} \text{ sr}^{-1}$  (Fadda et al. 2002; Elbaz et al. 2002).

(iv) Upper limits on the CIB at  $\lambda < 40 \mu\text{m}$  set by TeV cosmic opacity measurements toward blazars (Franceschini et al. 2001).

The above data are displayed in Fig. 3. We also show the expected cumulative quasar light spectrum in the near-infrared ( $\lambda < 1 \mu\text{m}$ ), calculated from the blue bump template, equation (14), with the normalization fixed by the cosmic X-ray background. Evidently only loose constraints can be obtained on the far-IR emission of the average quasar from the presented data alone. Fortunately, the radiative energy exchange between the quasar and the surrounding gas does not depend at all on the spectral shape at IR wavelengths. The only important thing is the total luminosity emitted in this spectral band, and it is possible to obtain some constraints on this quantity from the observational data presented in Fig. 3.

Indeed, it is widely accepted that the mechanism responsible for the IR emission of radio-quiet quasars (and partly for that of radio-loud quasars) is thermal radiation from radiatively heated dust (Barvainis 1987). Therefore, whichever is the spectral distribution of the IR emission from a quasar or from an ensemble of quasars, it cannot be narrower than that of modified black body emission from monotemperature dust:

$$F_E(\text{dust}) \propto \frac{E^{3+\beta}}{\exp(E/kT_d) - 1}, \quad (15)$$

where  $T_d$  is the dust temperature,  $\beta \sim 1\text{--}2$  is the emissivity index, and we have assumed the emission to be optically thin [the effect of a significant optical depth can be mimicked by varying the values of  $\beta$  and  $T_d$  in equation (15)].

We show in Fig. 3 several examples of spectra of the cumulative quasar light computed from equations (4)–(6) for the template spectrum (15) taking different  $T_d$  values. Normalizing the resulting spectra at 15  $\mu\text{m}$  to  $0.5 \text{ nW m}^{-2} \text{ sr}^{-1}$ , the current best estimate for  $EI_E$ , we can derive an upper

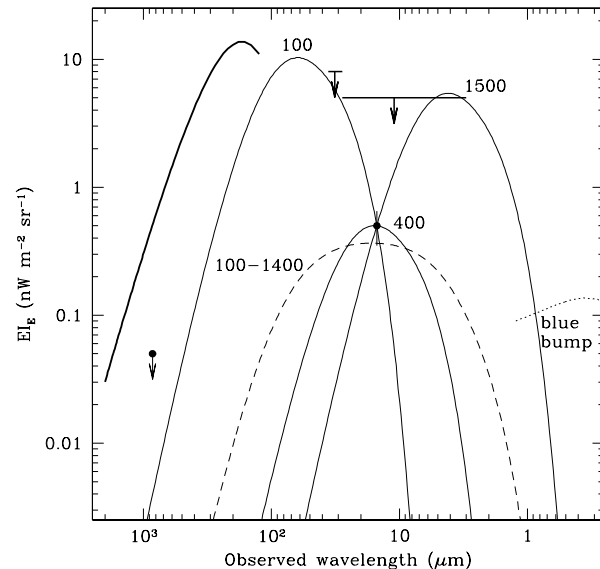


**Figure 3.** Observational constraints on the spectrum of cumulative AGN IR and submm light: the data point with error bars at 15  $\mu\text{m}$  and the upper limit at 850  $\mu\text{m}$ . Also shown are the COBE/FIRAS spectrum of the total extragalactic background (CIB) at 125–2000  $\mu\text{m}$  (thick solid line) and upper limits on the CIB at 3–40  $\mu\text{m}$ . See text for references to the data. All these data combined allow a large variety of possible IR spectra of the average quasar, including the modified black body emission spectrum, equation (15); the result of convolution of this model spectrum with the quasar evolution function, equations (4)–(6), is shown for  $\beta = 2$  and three values of the dust effective temperature (as indicated in K above the corresponding curves) that either maximize or minimize the integral  $EI_E$ . The additional integral constraint given by equation (22) leads to the adopted average quasar IR spectrum, equation (23) (dashed line, after convolution with the quasar evolution function). Also shown (dotted line) is the adopted average quasar spectrum in the blue bump region, equation (14), after convolution with the quasar evolution function, with the normalization fixed by the cosmic X-ray background.

limit on the integrated IR emission from quasars as a function of the characteristic dust temperature  $T_d$ . In this way we find that  $\int I_E dE < 15 \text{ nW m}^{-2} \text{ sr}^{-1}$  and  $< 8 \text{ nW m}^{-2} \text{ sr}^{-1}$  for  $T_d = 100$  and 1500 K, respectively. These limiting dust temperatures lead to maximal luminosities. The more general upper limit  $\int I_E dE \lesssim 20 \text{ nW m}^{-2} \text{ sr}^{-1}$  is applicable to any realistic spectral distribution, characterized by a range of  $T_d$ .

On the other hand, there is a more stringent, lower limit on the cumulative, frequency-integrated far-IR light from quasars:

$$I_{\text{IR}} \equiv \int_0^{1\text{eV}} I_E dE > 0.8 \pm 0.3 \text{ nW m}^{-2} \text{ sr}^{-1}. \quad (16)$$

This minimum corresponds to dust emission with  $T_d \approx 400$  K (see Fig. 3), and the quoted error results from the uncertainty in the observed flux of cumulative AGN light at 15  $\mu\text{m}$ .



Let us now derive an upper limit on  $I_{\text{IR}}$ , following the argument of Soltan (1982). The mass density of MBHs in the local universe is estimated as  $\rho_{\text{BH}} = (3 \pm 1) \times 10^5 M_{\odot} \text{ Mpc}^{-3}$  (Yu & Tremaine 2002; Aller & Richstone 2002), taking  $h = 0.72 \pm 0.05$  (Spergel et al. 2003). Assuming that all of this mass has been accumulated through accretion with a redshift-independent mass-to-radiation conversion efficiency  $\epsilon_{\gamma}$  gives an upper limit on the total, frequency-integrated radiation flux from all quasars:

$$I_{\text{total}} \equiv \int_0^{\infty} I_E dE \leq \frac{\epsilon_{\gamma} c^3 \rho_{\text{BH}}}{4\pi} \frac{\int e(z)/(1+z) |dt/dz| dz}{\int e(z) |dt/dz| dz} \approx (1.7 \pm 0.6) \frac{\epsilon_{\gamma}}{0.1} \text{ nW m}^{-2} \text{ sr}^{-1}, \quad (17)$$

where we have again used equation (6) to describe the quasar emissivity evolution (although the dependence of the result on  $e(z)$  is weak).

Now, the total flux  $I_{\text{total}}$  consists of contributions from the high-energy region ( $> 1$  keV), the blue-bump region ( $1 \text{ eV} < E < 1 \text{ keV}$ ) and the low-frequency region ( $< 1 \text{ eV}$ ). The first of these components can be found directly by integrating the CXGB spectrum shown in Fig. 1:

$$I_{\text{X-ray}} = 0.29 \pm 0.06 \text{ nW m}^{-2} \text{ sr}^{-1}, \quad (18)$$

where the quoted error has been propagated from the uncertainty in the CXGB normalization.

A more conservative estimate can be obtained by integrating the X-ray background over the 1–150 keV range, where it is certainly dominated by AGN emission:

$$I_{1-150 \text{ keV}} = 0.21 \pm 0.04 \text{ nW m}^{-2} \text{ sr}^{-1}, \quad (19)$$

The corresponding integral over the blue bump can be found by substituting the template given by equations (8) and (14) into equations (4)–(6), and using the normalization provided by the CXGB:

$$I_{\text{blue}} = 0.4_{-0.2}^{+0.4} \text{ nW m}^{-2} \text{ sr}^{-1}, \quad (20)$$

where we have roughly estimated the observational uncertainty in the average optical to soft-X-ray spectrum of type 1 quasars.

We can now estimate the maximum possible integrated quasar infrared ( $\lambda > 1$  mm) light:

$$I_{\text{IR}} = I_{\text{total}} - I_{\text{blue}} - I_{1-150 \text{ keV}} \leq (1.7 \pm 0.6) \frac{\epsilon_{\gamma}}{0.1} - 0.7 \pm 0.3 \text{ nW m}^{-2} \text{ sr}^{-1}. \quad (21)$$

One can see that the upper limit on  $I_{\text{IR}}$ , equation (21), is consistent with the lower limit on  $I_{\text{IR}}$ , equation (16), if  $\epsilon_{\gamma}$  is above 0.05, implying that MBHs have grown by radiatively efficient accretion via a standard disk. A similar conclusion was earlier reached by other researchers (e.g. Elvis et al. 2002; Yu & Tremaine 2002). If we additionally require that  $\epsilon_{\gamma} \leq 0.1$ , then we find from the limits given by equations (16) and (21) that

$$I_{\text{IR}} = (1.0 \pm 0.6) \text{ nW m}^{-2} \text{ sr}^{-1}. \quad (22)$$

It was implicit in the above treatment that the radiative output of quasars is purely the result of accretion onto MBHs. Recent observational data lend support to this view, seemingly excluding starburst activity as the dominant contributor to the bolometric luminosity of powerful AGN producing the bulk of the cosmic X-ray background.

Indeed, high-quality spectra obtained with the *ISO* satellite for dozens of optically bright quasars (Haas et al. 2000; Polletta et al. 2000; Andreani et al. 2003), plotted in units  $EF_E$ , exhibit a broad bump rising from 1–2  $\mu\text{m}$  (followed by the blue bump on the short-wavelength side) and declining in most cases at  $\lambda \gtrsim 60 \mu\text{m}$ . This bump is interpreted as multitemperature thermal emission from warm dust, with the maximum temperature (1000–1500 K) representing the evaporation temperature of dust grains. In addition, the far-IR spectra measured for several obscured quasars also tend to peak below 30  $\mu\text{m}$  (e.g. Barvainis et al. 1995; Deane & Trentham 2001).

The fact that the bulk of the infrared luminosity of quasars is emitted at wavelengths shorter than 60  $\mu\text{m}$  implies that dust cooler than  $\sim 50$  K is typically not energetically important. This, according to the standard theory (e.g. Rowan-Robinson 1995), suggests that the observed infrared emission is mostly the result of reprocessing by dust of the optical–UV radiation from the nucleus, rather than resulting from starburst activity.

Overall, the available data are consistent with the dominant contribution to the infrared luminosity of a typical quasar being due to dust heated to 50–1500 K by the radiation released as a result of accretion onto the central MBH. For this reason we consider equation (22) a robust estimate that can be used to normalize the average IR quasar spectrum, for which we adopt the following template:

$$\langle F_E \rangle = 1.5 \times 10^{42} \int_{100 \text{ K}}^{1400 \text{ K}} \frac{E^5 T_d^{-7}}{\exp(E/kT_d) - 1} dT_d, \quad E < 1 \text{ eV}, \quad (23)$$

where  $E$  and  $T_d$  are measured in keV and K, respectively.

This spectrum, which bears a greater resemblance to observed quasar spectra than equation (15), represents optically thin modified ( $\beta = 2$ ) black-body emission of dust characterized by a range of temperatures (100–1400 K) and constant emitted luminosity per unit logarithmic  $T_d$  interval (so that the spectrum has a flat core when plotted in  $EF_E$  units). The numerical coefficient in equation (23), which is defined relative to the X-ray component, equation (8), enables that  $\int_0^{1 \text{ eV}} I_E dE = 1.0 \text{ nW m}^{-2} \text{ sr}^{-1}$ . The adopted upper  $T_d$  value enables continuity at 1 eV between the distributions given by equations (23) and (14), while the lower  $T_d$  boundary and the spectral form have been chosen rather arbitrarily to allow the predicted cumulative quasar light to be consistent with the data point at 15  $\mu\text{m}$  (see Fig. 3).

### 3.4 The broad-band spectrum

We are now finally in a position to put together the different pieces of the average quasar spectrum. The resulting broad-band spectrum is shown in Fig. 4. It has three broad maxima in terms of energy output: one in the medium infrared, the blue bump and another one at  $\sim 60$  keV. It is necessary to note that the radio ( $\lambda > 1$  cm) component of the quasar spectrum is unimportant, because its contribution to the total energy output and consequently to the net Compton cooling rate is very small. This follows from the estimated surface brightness of the extragalactic radio background –  $\int I_E dE \sim 10^{-4} \text{ nW m}^{-2} \text{ sr}^{-1}$  (Bridle 1967; Dwek & Barker 2002) and also from spectroscopy of individual quasars – the radio luminosity of radio-quiet and radio-loud quasars

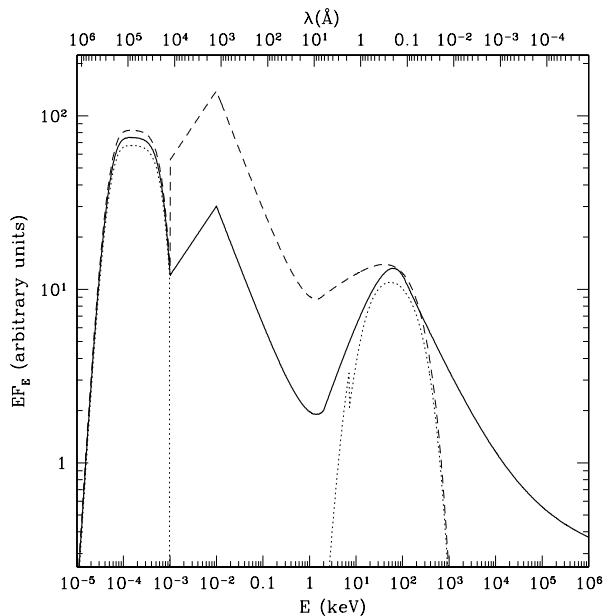


**Figure 4.** *Solid line:* Broad-band spectrum of the average quasar adopted in this paper. *Dashed line:* Adopted spectrum of the average unobscured quasar, rescaled by a factor of 1.1 for visibility. *Dotted line:* Adopted spectrum of the average obscured quasar, rescaled by a factor of 0.9. The weighted sum of the adopted type 1 and type 2 spectra (not shown) matches well the average spectrum below 300 keV.

is typically 3 and 5 orders of magnitude smaller, respectively, than the luminosity of the IR or blue bumps (e.g. Elvis et al. 1994). We note, however, that in the vicinity of parsec-scale quasar jets simulated Compton heating by their radio radiation can become important (Levich & Sunyaev 1971).

Since we shall study in the following sections the effect of AGN obscuration on gas heating and cooling, we show in Fig. 4 two additional spectra that may be considered representative of type 1 and type 2 quasars. We have defined these templates in a somewhat arbitrary manner, which is unavoidable for several reasons, in particular the distribution of emitted energy between the hard X-ray component and the blue bump may be intrinsically anisotropic, i.e. depend on the line of sight even in the absence of circumnuclear absorption; also the obscuration pattern may be more complicated than assumed, e.g. some quasars may appear obscured in the UV but unabsorbed in the X-ray, etc. Specifically we required that

- the ratio of obscured to unobscured quasars be 3 to 1,
- in the X-ray region, the type 1 and type 2 spectra be given by equation (9) and equation (10), respectively,
- the type 2 spectrum have no emission in the blue bump region,
- the infrared bump be the same for all three considered templates.

The weighted sum of the adopted obscured and unobscured quasar spectra matches well the globally averaged quasar spectrum below  $\sim 300$  keV. We recall that this upper bound-

ary results directly from the cutoff energy (200 keV) that we adopted in equation (9) and that there remains a significant observational uncertainty in the position of this cutoff for Seyfert galaxies and quasars.

#### 4 COMPTON TEMPERATURE

We can now determine the Compton temperature  $T_C$  characterizing the spectral output of the average quasar, which is the gas temperature at which Compton heating balances Compton cooling. An accurate result in the limit  $kT_C \ll m_e c^2 = 511$  keV can be obtained from equations given in Appendix by requiring that  $(dW/dt)_+ + (dW/dt)_- = 0$ .

Let us note here that if additionally  $E \ll m_e c^2$ , the Compton cooling rate becomes proportional to the frequency-integrated flux  $\int \langle F_E \rangle dE$ . We may thus expect that for our adopted average quasar spectrum most of the cooling will be provided by the infrared component, with additional smaller contributions coming from the optical-UV and high-energy bands. Klein-Nishina corrections act to further reduce the cooling by hard X-rays and gamma-rays. On the other hand, the Compton heating rate is, in the limit  $E \ll m_e c^2$ , proportional to another integral,  $\int E \langle F_E \rangle dE$ , which is completely dominated by the high-energy component of the quasar spectrum. However, also in this case Klein-Nishina corrections dramatically diminish the heating by photons with  $E \gtrsim 100$  keV.

Both the Compton heating and the Compton cooling integrals are well constrained for the adopted average quasar spectrum. First, the spectral shape of the high-energy component is known very well at least up to 300 keV and its normalization is uncertain to within  $\sim 20\%$  – see equation (18). Second, the uncertainty in the radiation flux integrated over the entire average spectrum is  $\sim 40\%$ , as follows from equations (16), (17) and (21). We can thus determine the characteristic Compton temperature quite accurately:

$$T_C = (1.9 \pm 0.8) \times 10^7 \text{ K}. \quad (24)$$

We emphasize that the surprisingly small uncertainty in the final result has resulted from three facts: 1) good knowledge of both the spectrum and normalization of the CXGB, 2) the lower limit on the cumulative AGN light in the infrared band that follows from the cross-correlation of deep X-ray and infrared surveys and 3) the upper limit on the total flux from all quasars inferred from the local density of MBHs. It is interesting that the detailed properties of the blue bump play a minor role in obtaining equation (24). Indeed, the contribution of the blue bump to the Compton heating rate is negligible, while its contribution to the Compton cooling rate is of the order of 25%, which is less than the uncertainty in the  $T_C$  value for the average quasar.

The value given by equation (24) corresponds to the entire spectrum extending into the gamma-ray band. If we exclude from consideration the spectral segment above 300 keV whose AGN origin still needs to be proven or disproven, we find

$$T_C(< 300 \text{ keV}) = 1.3 \times 10^7 \text{ K}. \quad (25)$$

Therefore, AGN emission above 300 keV contributes less than 30% to the total Compton heating rate (its contribution to the Compton cooling rate being negligible). The

contribution of emission above 500 keV is  $< 20\%$  and this excludes blazar beamed emission as a major contributor to the global heating due to AGN.

We can similarly calculate the Compton temperatures corresponding to the adopted type 1 and type 2 quasar spectra (see Fig. 4):

$$T_C(\text{unobsc}) = 0.8 \times 10^7 \text{ K}, \quad (26)$$

$$T_C(\text{obsc}) = 2.0 \times 10^7 \text{ K}. \quad (27)$$

Because we have taken substantial freedom in defining the type 1 and type 2 spectra, the above values are clearly more uncertain than the Compton temperature corresponding to the globally averaged spectrum.

We should note that the above calculation of Compton energy exchange is valid in the case of a Maxwellian momentum distribution of electrons, and thus assumes that the time scale for isotropization of electron momenta by mutual collisions is shorter than that for scattering of hard photons by electrons. We also explicitly assumed in our calculations that there is no significant bulk motion of the plasma caused by the gravity and radiation pressure of the central MBH. Both of these assumptions can be violated very close to quasar nuclei.

## 5 EFFECTS OF EXPOSING GAS TO THE RADIATION FROM THE AVERAGE QUASAR

Having built the spectrum and determined the characteristic Compton temperature of the average quasar, we can now estimate the consequences of exposing gas of cosmic chemical composition to the radiation from such sources.

### 5.1 Maximum distance of heating in the low density limit

As was noted in §1, it is well established that MBHs sitting in the centers of local galaxies have experienced an epoch or multiple epochs of rapid growth accompanied by the appearance of a quasar. One may therefore ask: to which maximum radius could a MBH currently of mass  $M_{\text{BH}}$  heat during its life time gas from a low initial temperature to the quasar Compton temperature? Such formulation assumes that the gas is of sufficiently low density that it is fully photoionized so that only Compton heating and cooling are important.

For gas of temperature  $T$  the heating rate per electron at a distance  $r$  from the quasar is

$$\frac{dW}{dt} = \frac{L(t)\sigma_T}{4\pi r^2} \frac{4k(T_C - T)}{m_e c^2}, \quad (28)$$

where  $L$  is the quasar luminosity, and we have assumed that the source is isotropic. Since the quasar is powered by accretion, the luminosity can be related to the rate of growth of the MBH:

$$L(t) = \epsilon_\gamma \frac{dM_{\text{BH}}}{dt}(t)c^2. \quad (29)$$

Hence, the total energy received during the growth of the MBH by an electron–proton pair located at  $r$  is

$$\Delta W = \frac{kT_C}{m_e c^2} \frac{\sigma_T}{\pi r^2} \epsilon_\gamma M_{\text{BH}} c^2, \quad (30)$$

assuming that  $T \ll T_C$ .

If we now require that each electron–proton pair receive an energy at least  $\Delta W = 3kT_C$ , we find the maximum distance out to which this can be done:

$$r_C = \left( \frac{\sigma_T \epsilon_\gamma M_{\text{BH}}}{2\pi m_e} \right)^{1/2} = 0.4 \text{ kpc} \left( \frac{\epsilon_\gamma}{0.1} \right)^{1/2} \left( \frac{M_{\text{BH}}}{10^8 M_\odot} \right)^{1/2}. \quad (31)$$

### 5.2 Heating/cooling of a partially ionized gas

Up to now our attention has been focused on Compton heating and cooling. However, gas exposed to intense quasar radiation may be sufficiently dense to remain only partially ionized. Photoionization heating as well as cooling through continuum and line emission will then be important. We consider this situation below.

We assume that the gas is optically thin and is in ionization equilibrium. Note that the characteristic ionization and recombination times are typically much shorter than the time scale for Compton heating/cooling. We adopt the solar element abundances from Grevesse, Noels & Sauval (1996), unless stated otherwise. Under these assumptions, the ionization balance as well as the heating and cooling rates are fully determined by the instantaneous gas temperature, the radiation spectral distribution and the ionization parameter (Tarter, Tucker & Salpeter 1969), which we define here as

$$\xi \equiv \frac{L_{\text{bol}}}{nr^2} = 1.4 \times 10^9 \frac{L_{\text{bol}}}{L_{\text{Edd}}} \frac{M_{\text{BH}}}{10^8 M_\odot} \frac{1 \text{ cm}^{-3}}{n} \left( \frac{1 \text{ pc}}{r} \right)^2, \quad (32)$$

where  $L_{\text{bol}}$  ( $\text{erg s}^{-1}$ ) is the bolometric, angular-integrated luminosity of the central source,  $L_{\text{Edd}}$  is the Eddington luminosity for a given MBH mass,  $n$  the hydrogen nucleus density and  $r$  the distance from the source. To proceed we assume that 3/4 of the whole sky as seen from the MBH is obscured while 1/4 is clear and that the emergent spectrum is described by either the adopted type 2 or type 1 spectrum (see Fig. 4), dependent on from which part of the sky the source is observed. According to this picture, observers located at the same distance but in different directions from the source will receive equal radiation fluxes above  $\sim 20$  keV and below  $\sim 1$  eV, but those looking through the obscuring torus will not see any optical, UV or soft X-ray radiation.

We performed computations using the latest version of XSTAR (Kallman 2002), to which we have added a block responsible for calculating Compton heating and cooling from equations (A1) and (A2). Our code also accounts for an additional heating caused by Compton scattering of hard X-rays off electrons bound in hydrogen and helium atoms. To this end we use the simple approximation that the Compton heating rate per electron is the same for bound and free electrons and is described by equation (A1). This implies that the net Compton heating rate per unit volume does not depend on the fraction of free electrons in the plasma, as opposed to the Compton cooling rate, which is proportional to this fraction. This has been shown to be a good approximation for photons with energies above a few keV (Basko, Sunyaev & Titarchuk 1974; Sunyaev & Churazov 1996), and such photons completely dominate the Compton heating in our case.

Since the definition of  $\xi$  adopted in XSTAR is different from ours, equation (32), we provide here the relations between  $L_{\text{bol}}$  and the ionizing flux  $F_{\text{ion}}$  (between 13.6 eV and

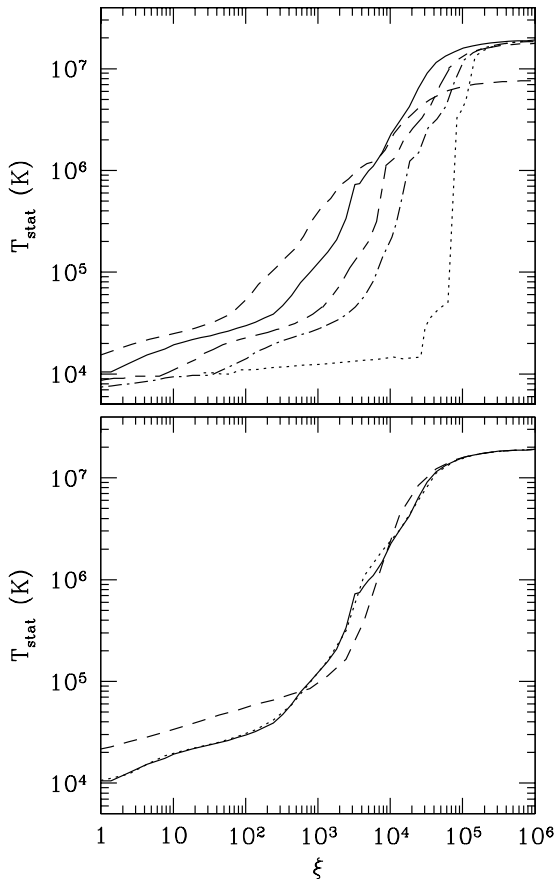


**Figure 5.** (a) Dependence on the ionization parameter, equation (32), of the stationary temperature of plasma of solar chemical composition exposed to the different radiation spectral distributions considered in this paper: the globally averaged quasar spectrum (solid line), type 1 spectrum (dashed line), type 2 spectrum (dotted line), and additionally  $\langle F_E \rangle(\text{type2}) + 0.01 \langle F_E \rangle(\text{type1})$  (dot-dashed line) and  $\langle F_E \rangle(\text{type2}) + 0.05 \langle F_E \rangle(\text{type1})$  (short-dash-long-dashed line). (b) The effect of plasma chemical composition on the  $T_{\text{stat}}(\xi)$  curve for the average quasar spectrum. *Solid line:* solar element abundances, *dotted line:* iron is absent, *dashed line:* H–He gas.

13.6 keV) in obscured and unobscured directions as well as its average over the sky:

$$\begin{aligned} \frac{\langle 4\pi r^2 F_{\text{ion}} \rangle}{L_{\text{bol}}} &= 0.13, \\ \frac{4\pi r^2 F_{\text{ion}}(\text{unobsc})}{L_{\text{bol}}} &= 0.50, \quad \frac{4\pi r^2 F_{\text{ion}}(\text{obsc})}{L_{\text{bol}}} = 0.012. \end{aligned} \quad (33)$$

Suppose now that the irradiated gas has had enough time to achieve thermal equilibrium. Fig. 5a shows the gas stationary temperature  $T_{\text{stat}}$  as a function of  $\xi$  for each of the different spectral templates presented in Fig. 4. Fig. 5b illustrates the effect of gas enrichment by metals and iron on the  $T_{\text{stat}}(\xi)$  curve. We see that the gas reaches the Compton temperature given by equations (24)–(27) when  $\xi \gtrsim 10^5$ . In this region the gas is fully photoionized and the ther-

mal balance is dominated by Compton heating and cooling. At  $\xi \lesssim 10^5$ , the  $T_{\text{stat}}(\xi)$  curves are fairly similar for the globally averaged spectrum and for the type 1 spectrum, and are mainly determined by the balance between photoionization heating and various cooling mechanisms (see Kallman & McCray 1982 for a detailed discussion of the underlying physics).

Therefore, for given luminosity  $L_{\text{bol}}$  and gas radial distribution  $n(r)$ ,  $r(\xi = 10^5)$  defines the size of a Compton heating zone where gas can achieve a steady state with  $T = T_C$ . Consider as a specific example M87, a giant elliptical galaxy in the Virgo cluster. M87 hosts a  $3 \times 10^9 M_\odot$  MBH and contains hot ( $T \sim 10^7$  K) gas characterized by  $n \sim 0.1, 0.05$  and  $0.02 \text{ cm}^{-3}$  at  $r = 1, 4$  and  $10$  kpc, respectively (Matsushita et al. 2002). For these parameters, the outer boundary of the Compton heating zone would be at  $r(10^5) \approx 1$  kpc if the M87 nucleus switched on at its Eddington luminosity. This size is somewhat smaller than  $r_C = 2.2$  kpc given by equation (31) for M87.

The  $T_{\text{stat}}(\xi)$  curve is quite different for  $\xi < 10^5$  in the case of the type 2 spectrum, for almost complete lack of ionizing UV and soft X-ray photons. In this case, there is a narrow transition region at  $\xi \sim 10^5$  dividing a high-temperature and low-temperature regions characterized by  $T_{\text{stat}} = T_C \sim 10^7$  and  $\sim 10^4$  K, respectively. Moreover, the solution in this transition zone is known to be unstable (e.g. Buff & McCray 1974; Kallman & McCray 1982). It is interesting to note that in the low-temperature region, where the gas is practically neutral, Compton heating due to scattering on bound electrons contributes 8% to the total heating rate dominated by photoionization of metallic atoms by hard X-rays. This, however, has negligible effect (less than 1%) on the resulting equilibrium temperature in the low-temperature region. The effect is even smaller for the average and type 1 quasar spectra, in which case the photoionization heating associated with the radiation above 13.6 eV is several orders of magnitude stronger than Compton heating on bound electrons in the low-ionization limit ( $\xi \lesssim 10^{-4}$ ).

The results presented in Fig. 5a thus imply that radiative heating can be quite different for  $\xi \lesssim 10^5$ , i.e. outside the Compton heating zone, if plasma is exposed to the radiation reprocessed by the obscuring torus instead of being irradiated directly by the quasar nucleus. The direct consequence of this is the possibility of significantly anisotropic radiative feedback on the quasar environment in the scenario with partial obscuration of the nucleus: strong photoionization heating (of an initially cold material) can take place within the cones of direct nuclear emission but not in obscured directions.

We, however, consider the above situation unlikely, because it resulted from the complete absence of UV and soft X-ray radiation in our adopted type 2 spectrum. In reality the heating anisotropy will be significantly reduced if a small fraction of the ionizing radiation outgoing from the nucleus within the open cones is scattered into obscured lines of sight. This is demonstrated by computations we performed for input spectra given by  $\langle F_E \rangle(\text{type2}) + 0.01 \langle F_E \rangle(\text{type1})$  and  $\langle F_E \rangle(\text{type2}) + 0.05 \langle F_E \rangle(\text{type1})$ . This corresponds to the scattering gas having a Thomson optical depth of  $\tau_T \sim 0.04$  and  $\sim 0.2$ , respectively, assuming that this gas is ionized (so that electron scattering of UV radiation is possible) and fills

the central funnel of the torus and extends some distance above its top, covering at least  $f = 1/4$  of the sky as seen from the nucleus. As can be seen from Fig. 5a, the addition of such a small amount of scattered ionizing radiation changes the situation dramatically, significantly diminishing the departure of the resulting  $T_{\text{stat}}(\xi)$  curve from those corresponding to the globally averaged and type 1 spectra. In such a case, irradiation by the quasar will probably have rather similar effects on gas located along unobscured and obscured lines of sight not only inside the zone governed by Compton heating and cooling but also outside it.

Different kinds of observation do reveal significant quantities of warm ( $T \sim 10^{4.5} - 10^6$  K) ionized gas located at distances from possibly a fraction of a pc up to hundreds of pc from the nuclei of Seyfert galaxies (e.g. Krolik & Kriss 2001). In Seyfert 2 galaxies such as NGC 1068, this plasma reveals itself via polarized scattered emission in the optical (e.g. Miller & Goodrich 1990) and via scattered continuum, recombination emission and resonance scattering in the X-ray band (e.g. Turner et al. 1997; Ogle et al. 2003). The same photoionized gas produces absorption features in the UV and soft X-ray spectra of Seyfert 1 galaxies and some quasars (e.g. George et al. 1998; Mathur et al. 1994). Further,  $\sim 10\%$  of optically selected quasars show broad absorption lines (BALs), arising in material apparently flowing outward from the nucleus with velocities  $\sim 10^4$  km s $^{-1}$ , and it appears that most or possibly all quasars contain such BAL outflows (e.g. Green et al. 2001). Finally, powerful radio galaxies at high redshifts show strong UV line and continuum emission extended along the axis of the radio source, which is interpreted as scattered radiation from an obscured quasar nucleus (e.g. Tran et al. 1998). Taken together, all these diverse observations suggest that a warm or hot gas characterized by the product  $\tau_{\text{T}} f \lesssim$  a few per cent – of the same order as the scattering fractions assumed in our simulations above – may be ubiquitously present in AGN. We also note that electron scattering optical depths  $\tau_{\text{T}} \sim$  several  $10^{-2}$  are predicted for the  $\sim 100$  pc cooling flows feeding quasars in elliptical galaxies (e.g. Ciotti & Ostriker 2001).

We finally note that the  $T_{\text{stat}}(\xi)$  curves shown in Fig. 5 descend below  $10^4$  K when  $\xi$  becomes less than  $\sim 1$ . This implies that the gas density must exceed  $10^7$  cm $^{-3}$  ( $10$  pc/ $r$ ) $^2$  at distance  $r$  from a  $10^8 M_{\odot}$  black hole radiating at Eddington limit in order to provide conditions for the existence of a dusty molecular torus such as postulated in the AGN unification model. Such dense material cannot fill more than a small fraction of the obscuration region, otherwise its large Thomson optical depth  $\tau_{\text{T}} > 2 \times 10^2$  ( $10$  pc/ $r$ ) will prevent even hard X-rays from escaping through the torus and make the source Compton thick. We note that XSTAR becomes unsuitable at  $T \lesssim 3000$  K.

## 6 CONCLUSIONS

The main results obtained in this work are as follows.

We combined information on the cumulative AGN light in the IR and X-ray bands, the estimate of the local mass density of MBHs and composite optical to soft X-ray quasar spectra to construct in a robust way the angular-integrated radiation spectrum of the average quasar in the universe

(§3). This spectrum characterizes the global energy release via accretion onto MBHs, and is the result of implicit summing over unobscured and obscured sources.

We calculated (§4) the Compton heating and cooling rates for gas exposed to radiation with the adopted average quasar spectral distribution. The Compton heating results from downscattering in energy of the hard X-rays, while the cooling is due to inverse Compton scattering of primarily the IR photons. The Compton temperature, representing the equilibrium between Compton heating and cooling, is well constrained near  $2 \times 10^7$  K, with an estimated uncertainty in this value of  $\sim 50\%$ .

We presented simple arguments (§2) and supported them with accurate calculations (§4) that circumnuclear obscuration cannot significantly affect the Compton heating and cooling rates. As a result, the Compton temperatures characteristic of obscured and unobscured directions (or sources) are within a factor of 2 from the average  $T_{\text{C}}$  value quoted above.

The almost invariant shape of the (unabsorbed) hard X-ray spectrum combined with the recently published data of observations of tens and hundreds of optically bright quasars that cover the blue bump segment of the spectrum up to its connection with the X-ray component suggest that the rms source-to-source scatter in the ratio of the amplitudes of the hard X-ray and blue bumps is fairly small,  $\sim 2$ , at least for type 1 quasars. Of the same order is the possible trend going from relatively low-luminosity ( $L_{\text{X}} \sim 10^{44}$  erg s $^{-1}$ ) to high-luminosity ( $L_{\text{X}} \sim 10^{46}$  erg s $^{-1}$ ) quasars (§3.2). We thus believe that the average spectrum and Compton temperature found in this work should also represent well the spectral output of individual quasars, at least of their majority. We note that the IR emission from quasars results from reprocessing of the primary UV emission, so that both components always have comparable powers, and therefore the variability of the shape of the IR spectral component from source to source has practically no effect on this conclusion.

Bazar-type beamed emission is energetically unimportant globally, contributing on average less than 20% to the net Compton heating rate (§3.1.2). Nevertheless, current observations do not rule out the possibility that this additional radiation component can play an important role in gas heating for particular objects. This question needs further study.

We showed (§5.1) that during its lifetime a MBH of mass  $M_{\text{BH}}$  can heat to the Compton temperature low-density gas within a radius of  $\sim 0.5$  kpc ( $M_{\text{BH}}/10^8 M_{\odot}$ ) $^{1/2}$ , which would normally constitute a significant fraction of the effective radius of the spheroid in which the MBH resides and a negligible fraction of the core radius of a cluster of galaxies.

We performed computations (§5.2) of the radiative heating of partially photoionized plasma of cosmic chemical composition exposed to the radiation from the average quasar, taking into account photoionization heating and plasma cooling through line and continuum emission in addition to Compton heating and cooling. Although the derived  $T_{\text{stat}}(\xi)$  curves are quite different for the adopted obscured and unobscured spectra, we demonstrated that scattering of a relatively small fraction ( $\sim$  a few %) of the primary nuclear radiation by dense gas in the vicinity of the active nucleus will wipe away most of this difference. Observations indicate that such scattering does occur in most AGN. There-

fore, circumnuclear obscuration probably can be ignored to first order in considering the radiation feedback of MBHs on their environment.

The general results of this work provide us with the basis for follow-up work aimed at accurately calculating the feedback effect of MBHs on their gaseous environment.

## APPENDIX A:

In the limit  $kT \ll m_e c^2 = 511$  keV, the characteristic rates per electron of plasma heating and cooling due to spontaneous Compton scattering are given by (Shestakov et al. 1988; Sazonov & Sunyaev 2001)

$$\begin{aligned} \left(\frac{dW}{dt}\right)_+ &= \sigma_T m_e c^3 \\ &\int_0^\infty \epsilon_E(x) \left[ \frac{3}{8x^3} (x-3)(x+1) \ln(2x+1) \right. \\ &\quad \left. + \frac{-10x^4 + 51x^3 + 93x^2 + 51x + 9}{4x^2(2x+1)^3} \right] dx \\ &= \sigma_T m_e c^3 \\ &\int_0^\infty x \epsilon_E(x) \left[ 1 - \frac{21x}{5} + O(x^2) \right] dx \quad (\text{A1}) \end{aligned}$$

and

$$\begin{aligned} \left(\frac{dW}{dt}\right)_- &= -\sigma_T c k T \\ &\int_0^\infty \epsilon_E(x) \left[ \frac{3(3x^2 - 4x - 13)}{16x^3} \ln(2x+1) \right. \\ &\quad \left. + \frac{-216x^6 + 476x^5 + 2066x^4 + 2429x^3}{8x^2(2x+1)^5} \right. \\ &\quad \left. + \frac{1353x^2 + 363x + 39}{8x^2(2x+1)^5} \right] dx \\ &= -4\sigma_T c k T \\ &\int_0^\infty \epsilon_E(x) \left[ 1 - \frac{47x}{8} + O(x^2) \right] dx, \quad (\text{A2}) \end{aligned}$$

where  $x = E/m_e c^2$  and  $\epsilon_E(x)$  is the radiation spectral energy density. It follows that  $a(E) = 1 - 21E/5m_e c^2 + \dots$  and  $b(E) = 1 - 47E/8m_e c^2 + \dots$  in equations (1) and (2).

## REFERENCES

- Aller M.C., Richstone D., 2002, *AJ*, 124, 3035  
 Almaini O., Lawrence A., Boyle B.J., 1999, *MNRAS*, 305, L59  
 Andreani P., Cristiani S., Grazian A., La Franca F., Goldschmidt P., 2003, *AJ*, 125, 444  
 Antonucci R., 1993, *ARA&A*, 31, 473  
 Barger A.G., Cowie L.L., Brandt W.N., Capak P., Garmire G.P., Hornschemeier A.E., Steffen A.T., Wehner E.H., 2002, *AJ*, 124, 1839  
 Barvainis R., Antonucci R., Hurt T., Coleman P., Reuter H.-P., 1995, *ApJ*, 451, L9  
 Barvainis R., 1987, *ApJ*, 320, 537  
 Basko M.M., Sunyaev R.A., Titarchuk L.G., 1974, *A&A*, 31, 249  
 Binney J., Tabor G., 1995, *MNRAS*, 276, 663  
 Blom J.J. et al., 1995, *A&A*, 298, L33  
 Boyle B.J., Shanks T., Croom S.M., Smith R.J., Miller L., Loaring N., Heymans C., 2000, *MNRAS*, 317, 1014  
 Bridle A.H., 1967, *MNRAS*, 136, 219  
 Buff J. & McCray R., 1974, *ApJ*, 189, 147  
 Chiang J., Mukherjee R., 1998, *ApJ*, 496, 752  
 Ciotti L., Ostriker J.P., 1997, *ApJ*, 487, L105  
 Ciotti L., Ostriker J.P., 2001, *ApJ*, 551, 131  
 Cirasuolo M., Magliocchetti M., Celotti A., Danese L., 2003, *MNRAS*, 341, 993  
 Comastri A., Setti G., Zamorani G., Hasinger G., 1995, *A&A*, 296, 1  
 Comastri A., Di Girolamo T., Setti G., 1996, *A&AS*, 120, 627  
 Cowie L.L., Ostriker J.P., Stark A.A., 1978, *ApJ*, 226, 1041  
 Cowie L.L., Barger A.J., Bautz M.W., Brandt W.N., Garmire G.P., 2003, *ApJ*, 584, L57  
 Dwek E., Barker M.K., 2002, *ApJ*, 575, 7  
 Deane J.R., Trentham N., 2001, *MNRAS*, 326, 1467  
 della Ceca R., Lamorani G., Maccararo T., Wolter A., Griffiths R., Stocke J.T., Setti G., 1994, *ApJ*, 430, 533  
 Elbaz D., Cesarsky C.J., Chanial P., 2002, *A&A*, 384, 848  
 Elvis M. et al., 1994, *ApJ*, 95, 1  
 Elvis M., Risaliti G., Zamorani G., 2002, *ApJ*, 565, L75  
 Eracleous M., Sambruna R., Mushotzky R.F., 2000, *ApJ*, 537, 654  
 Fabian A.C., Iwasawa K., 1999, *MNRAS*, 303, L34  
 Fabian A.C., Smail I., Iwasawa K., 2000, *MNRAS*, 315, L8  
 Fadda D., Flores H., Hasinger G., 2002, *A&A*, 383, 838  
 Fan X. et al., 2001, *ApJ*, 121, 54  
 Fixsen D.J., Dwek E., Mather J.C., Bennett C.L., Shafer R.A., 1998, *ApJ*, 508, 123  
 Fossati G., Maraschi L., Celotti A., Comastri A., Ghisellini G., 1998, *MNRAS*, 299, 433  
 Franceschini A., Aussel H., Cesarsky C.J., Elbaz D., Fadda D., 2001, *A&A*, 378, 1  
 George I.M., Turner T.J., Netzer H., Nandra K., Mushotzky R.F., Yaqoob T., 1998, *ApJS*, 114, 73  
 Gilli R., Salvati M., Hasinger G., 2001, *A&A*, 366, 407  
 Gondek D., Zdziarski A.A., Johnson W.N., George I.M., McNaron-Brown K., Magdziarz P., Smith D., Gruber D.E., 1996, *MNRAS*, 282, 646  
 Grandi P., Urry C.M., Maraschi L., 2002, *New Astron. Rev.*, 46, 221  
 Green P.J., Aldcroft T.L., Mathur S., Wilkes B.J., Elvis M., 2001, *ApJ*, 558, 109  
 Grevesse N., Noels A., Sauval A., 1996, in ‘‘Cosmic Abundances’’ ASP Conference Series, 99, eds. S. Holt & G. Sonneborn, p. 117  
 Gruber D.E., Matteson J.L., Peterson L.E., Jung G.V., 1999, *ApJ*, 520, 124  
 Haas M uller S.A.H., Chini R., Meisenheimer K., Klaas U., Lemke D., Kreysa E., Camenzind M., 2000, *A&A*, 354, 453  
 Hasenkopf C.A., Smabruna R.M., Eracleous M., 2002, *ApJ*, 575, 127  
 Hasinger G. et al., 2001, *A&A*, 365, L45  
 Hasinger G., 2003, in ‘‘High Energy Processes and Phenomena in Astrophysics’’ IAU Symposium, 214, eds. X. Li, Z. Wang & V. Trimble; astro-ph/0301040  
 Ivezić Z. et al., 2002, *AJ*, 124, 2364  
 Iwasawa K., Fabian A.C., Ettore S., 2001, *MNRAS*, 321,

- L15
- Jourdain E. et al., 1992, *A&A*, 256, L38
- Kallman T.R., 2002, XSTAR Manual, version 2.1 (Greenbelt, MD: NASA/GSFC)
- Kallman T.R., McCray R., 1982, *ApJS*, 50, 263
- Koratkar A., Blaes O., 1999, *PASP*, 111, 1
- Krolik J.H., Kriss, G.A., 2001, *ApJ*, 561, 684
- Kubo H., Takahashi T., Madejski G., Tashiro M., Makino F., Inoue S., Takahara F., 1998, *ApJ*, 504, 693
- La Franca F. et al., 2002, *ApJ*, 570, 100
- Laor A., Fiore F., Elvis M., Wilkes B.J., McDowell J.C., 1997, *ApJ*, 477, 93
- Lawson A.J., Turner M.J.L., 1997, *MNRAS*, 288, 920
- Levich E.V., Sunyaev R.A., 1971, *Sov. Astron.*, 15, 363
- Madau P., Ghisellini G., Fabian A.C., 1994, *MNRAS*, 270, 17
- Maiolino R., Rieke G.H., 1995, *ApJ*, 454, 95
- Mathur S., Wilkes B., Elvis M., Fiore F., 1994, *ApJ*, 434, 493
- Matsushita K., Belsole E., Finoguenov A., Boehringer H. 2002, *A&A* 386, 77
- Matt G., Pompilio F., La Franca F., 1999, *New A*, 4, 191
- McNaron-Brown K. et al., 1995, *ApJ*, 451, 575
- Miller J.S., Goodrich R.W., 1990, *ApJ*, 355, 456
- Miyaji T., Ishisaki Y., Ogasaka Y., Ueda Y., Freyberg M.J., Hasinger G., Tanaka Y., 1998, *A&A*, 334, L13
- Miyaji T., Hasinger G., & Schmidt M., 2000, *A&A*, 353, 25
- Morrison R., McCammon D., 1983, *ApJ*, 270, 119
- Mukherjee R. et al., 1997, *ApJ*, 490, 116
- Norman C. et al., 2002, *ApJ*, 571, 218
- Ogle P.M., Brookings T., Canizares C.R., Lee J.C., Marshall H.L., 2003, *A&A*, 402, 849
- Orr A., Barr P., Guainazzi M., Parmar A.N., Young A.J., 2001, *A&A*, 376, 413
- Ostriker J.P., Weaver R., Yahil A., McCray R., 1976, *ApJ*, 208, L61
- Ostriker J.P., Steinhardt P.J., 1995, *Nature*, 377, 600
- Park M.G., Ostriker J.P., 2001, *ApJ*, 549, 100
- Perola G.C., Matt G., Cappi M., Fiore F., Guainazzi M., Maraschi L., Petrucci P.O., Piro L., 2002, *A&A*, 389, 802
- Polletta M., Courvoisier T.J.-L., Hooper E.J., Wilkes B.J., 2000, *A&A*, 362, 75
- Reeves J.N., Turner M.J.L., 2000, *MNRAS*, 316, 234
- Revnivtsev M., Gilfanov M., Sunyaev R., Jahoda K., Markwardt C., 2003, *A&A* (in press); astro-ph/0306569
- Risaliti G., Maiolino R., Salvati M., 1999, *ApJ*, 522, 157
- Risaliti G., Elvis M., Gilli R., 2002, *ApJ*, 566, L67
- Rosati P. et al., 2002, *ApJ*, 566, 667
- Rowan-Robinson M., 1995, *MNRAS*, 272, 737
- Ruiz-Lapuende P., Cassé M., Vangioni-Flam E., 2001, *ApJ*, 549, 483
- Salucci P., Szuszkiewicz E., Monaco P., Danese L., 1999, *MNRAS*, 307, 637
- Sazonov S.Yu., Sunyaev R.A., 2001, *Astron. Lett.*, 27, 481
- Schmidt M., Schneider D.P., Gunn J.E., 1995, *AJ*, 110, 68
- Schönfelder V., 1994, *ApJS*, 92, 593
- Severgnini P. et al., 2000, *A&A*, 360, 457
- Shestakov A.I., Kershaw D.S., Prasad M.K., 1988, *J. Quant. Spectrosc. Radiat. Transfer*, 40, 577
- Soltan A., 1982, *MNRAS*, 200, 115
- Spergel D.N. et al., 2003, *ApJS*, 148, 175
- Sreekumar P. et al., 1998, *ApJ*, 494, 523
- Staubert R., Maisack M., 1996, *A&A*, 305, L41
- Stern D., Djorgovski S.G., Perley R.A., de Carvalho R.R., Wall J.V., 2000, *AJ*, 119, 1526
- Stern D. et al., 2002, *ApJ*, 568, 71
- Sunyaev R.A., 1978, *Sov. Astron. Lett.*, 4, 39
- Sunyaev R.A., Churazov E.M., 1996, *Astron. Lett.*, 22, 648
- Tarter C.B., Tucker W.H. & Salpeter E.E., 1969, *ApJ*, 156, 943
- Tavecchio F. et al., 2002, *ApJ*, 575, 137
- Telfer R.C., Zheng W., Kriss G.A., Davidsen A.F., 2002, *ApJ*, 565, 773
- The L.-S., Leising M.D., Clayton D.D., 1993, *ApJ*, 403, 32
- Tran H.D., Cohen M.H., Ogle P.M., Goodrich R.W., Alighieri S. di S., 1998, *ApJ*, 500, 660
- Tremaine S., 2002, *ApJ*, 574, 740
- Turner T.J., George I.M., Nandra K., Mushotzky R.F., 1997, *ApJ*, 488, 164
- Urry C.M., Padovani P., 1995, *PASP*, 107, 803
- Vanden Berk D.E. et al., 2001, *AJ*, 122, 549
- Vignali C., Brandt W.N., Schneider D.P., 2003, *AJ*, 125, 433
- Woźniak P.R., Zdziarski A.A., Smith D., Madejski G.M., Johnson W.N., 1998, *MNRAS*, 299, 449
- Yu Q., Tremaine S., 2002, *ApJ*, 335, 965
- Yuan W., Brinkmann W., Siebert J., Voges W., 1998, *A&A*, 330, 108
- Zdziarski A.A., 1996, *MNRAS*, 281, L9